JOURNAL OF
Materials
CHEMISTRY

Synthesis and macroscopic second-order nonlinear optical properties of poly(ether imide)s containing a novel two-dimensional carbazole chromophore with nitro acceptors

Wen-Jang Kuo,[a] Ging-Ho Hsiue*[a,b] and Ru-Jong Jeng[b]

[a]*Department of Chemical Engineering, National Tsing Hua University, Hsinchu, Taiwan, 300, ROC. E-mail: ghhsiue@che.nthu.edu.tw; Fax: 886-3-5726-825*
[b]*Department of Chemical Engineering, National Chung Hsing University, Taichung, Taiwan, 402, ROC*

Received 30th July 2001, Accepted 19th December 2001
First published as an Advance Article on the web 20th February 2002

Taking advantage of the multifunctional characteristics of carbazole along with rational molecular design, a two-dimensional carbazole chromophore with strong nitro acceptors was synthesized by a facile synthetic route. A first molecular hyperpolarizability of 163×10^{-30} esu was acquired through solvatochromic methods. By doping of the chromophores into an organosoluble poly(ether imide), a series of guest–host NLO polymers were acquired. A high doping level up to 20 wt% was obtained without observing aggregation of NLO chromophores. The compatibility between chromophore and poly(ether imide) was also investigated by SEM and extraction experiments. In terms of compatibility, the molecular weight distribution of the polymer plays an important role. The second harmonic coefficients (d_{33}) for the NLO-active poly(ether imide)s range from 7 to 23 pm V^{-1} depending on the doping level. The effect of two-dimensional structure on the NLO temporal stability was investigated by tracing the second harmonic coefficient as a function of time. Moreover, the relaxation behavior of the NLO systems was further examined by dielectric analysis. Large rotational cone volumes give the two-dimensional chromophore excellent orientational stability when the temperature approaches the glass transition temperature observed from DEA.

Introduction

Organic second-order nonlinear optical (NLO) polymers are very promising for optoelectronic applications because of their inexpensive, easy to make, good film forming properties for waveguide fabrication, and compatibility with semiconductor technology.[1–3] These NLO polymers could be acquired *via* doping NLO chromophores into amorphous polymer matrices[4] or covalently incorporating NLO moieties onto a polymer backbone.[5–7] Most of the attempted chromophores are designed as one-dimensional charge transfer molecules. Such chromophores are represented as D–π–A, where the electron-donor (D) and electron-acceptor (A) groups are linked by a π-conjugated bridge.[8,9] In 1992, Yamamoto[10] developed a series of two-dimensional (2D) chromophores based on the charge transfer concept. These chromophores provide not only a better phase-matching property but also noncentrosymmetric crystal structures.

Guest–host NLO systems are highly accessible for studying the macroscopic NLO properties of the polymers despite the limitation of the temporal stability of the oriented dipole and miscibility between chromophores and polymers.[11–14] Aromatic polyimides are excellent candidates for NLO applications because of their robust mechanical properties and high thermal and chemical resistance. However, polyimides were somewhat restricted for guest–host NLO systems because of sublimation and decomposition of the chromophores during the imidization process. To circumvent these shortcomings, utilization of organosoluble polyimides seems to be a reasonable approach. Structural modification includes incorporation of flexible bridging linkages,[15–19] disrupting symmetry and regularity of the polymer backbone[15–21] and aromatic ether linkages into aromatic polymer backbone.

In this work, carbazole derivatives were chosen as the basic building chromophores because of their multifunctional properties, such as second-order NLO and photoconductive properties.[22–25] Moreover, the isoelectronic structures between the 3 and 6 positions enable carbazole easily to form a two-dimensional structure. Fig. 1 shows the chemical structure of the two-dimensional chromophore $Cz2PhNO_2$. First-order molecular hyperpolarizability (β_{xxx}) of the chromophore was calculated through solvatochromic methods. Moreover, an organosoluble poly(ether imide), 6FPEI (Fig. 1), served as the polymeric matrices for the NLO chromophores. By doping the

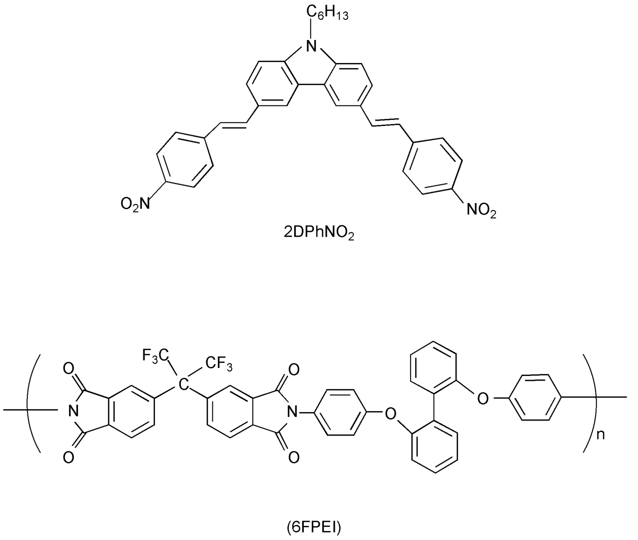

Fig. 1 Chemical structure of the chromophore $Cz2PhNO_2$ and the poly(ether imide) 6FPEI.

DOI: 10.1039/b106915m

chromophore into the poly(ether imide) with various contents, a series of guest–host NLO systems were acquired. A systematic investigation of variation of the chromophore contents on NLO properties has been pursued. The compatibility between chromophores and polymer matrix was also studied by SEM and extraction experiments. The two-dimensional chromophore effect on the nonlinear optical properties was investigated by temporal relaxation behavior and dielectric analysis.

Experimental

Materials

Chemicals such as carbazole, 1-bromohexane (Acros Organic Company), $POCl_3$ (Lancaster company), *p*-nitro-α-bromotoluene (Tokyo Kasei Kogyo Co., Ltd), triethyl phosphite (STREM Chemicals), biphenyl-2,2′-diol (Acros Organic Company) and hydrazine monohydrate (from Lancaster company) were used as received. Solvents such as *N*-methyl-2-pyrrolidone (NMP), *N*,*N*-dimethylacetamide (DMAc), *N*,*N*-dimethylformamide (DMF), and tetrahydrofuran (THF) were purchased from Tedia Company Inc. NMP, DMAc and DMF were dried over calcium hydride, and distilled under vacuum. THF was dried over sodium, and distilled.

Synthesis of the two-dimensional chromophore Cz2PhNO$_2$. *9-Hexylcarbazole.* A solution of carbazole (20 g; 120 mmol) in dry DMAc (50 mL) was added dropwise to suspended sodium hydride (5.8 g, 60 wt% in mineral oil; 145 mmol) in dry DMAc(50 mL) under nitrogen atmosphere at 0 °C for a period of 30 min. After addition of 1-bromohexane (30 g; 180 mmol), the solution was stirred for 6 hours at room temperature. De-ionised water was added to destroy sodium hydride, and the solution was extracted with ethyl acetate several times. After the extract was washed with de-ionised water, the extract was concentrated. Further purification was performed with column chromatography (pure *n*-hexane as eluent). ^{1}H NMR ($CDCl_3$): δ 0.85 (t, 3H, –CH_3), 1.32 (m, 6H, –CH_2–), 1.85 (quintet, 2H, –N–CH_2–CH_2–), 4.28 (t, 2H, –N–CH_2–), 7.22 (t, 2H, Ar–*H*, *para* to NH), 7.38 (d, 2H, Ar–*H*, *ortho* to NH), 7.45 (t, 2H, Ar–*H*, *meta* to NH), 8.08 (d, 2H, Ar–H, *ortho* to NH).

*9-Hexyl-3,6-diformyl-9*H*-carbazole.* DMF (30 g) was added dropwise to $POCl_3$ solution under 0 °C. A solution of 9-hexylcarbazole in 1,2-dichloroethane (50 mL) was then added. The reaction mixture was subsequently heated to 100 °C and kept stirring at this temperature for 24 h. When the reaction was completed, the reaction solution was added to cool NaOH aqueous solution (5%) and then extracted with dichloromethane several times. The organic layer was separated, washed with de-ionised water three times, dried over anhydrous magnesium sulfate, and concentrated under vacuum. Further purification was performed by column chromatography. Mp 131 °C. ^{1}H NMR ($CDCl_3$): δ 0.78 (t, 3H, –CH_3), 1.19 (m, 6H, –CH_2–), 1.82 (quintet, 2H, N–CH_2–CH_2–), 4.28 (t, 2H, –CH_2–), 7.44 (d, 2H, Ar–*H*, *ortho* to NH), 7.98 (d, 2H, Ar–*H*, *ortho* to CHO), 8.55 (s, 2H, Ar–*H*, *ortho* to CHO), 10.04 (s, 2H, C*H*O).

Diethyl (4-nitrobenzyl)phosphonate. Triethyl phosphite (11.53 g, 69.4 mmol) was added to *p*-nitro-α-bromotoluene (10 g, 43.6 mmol). The mixed solution was heated to 130 °C for 4 hours. Excess triethyl phosphite was removed by a rotary aspirator. Further purification was performed by column chromatography. ^{1}H NMR ($CDCl_3$): δ 1.19 (t, 6H, –CH_3), 3.15 (d, 2H, J = 22.28, Ph–CH_2–P(O)), 3.98 (q, 4H, P(O)–OCH_2–), 7.39 (d, 2H, Ar–*H*, *meta* to NO_2), 8.09 (d, 2H, Ar–*H*, *ortho* to NO_2).

*9-Hexyl-3,6-bis[2′-(4″-nitrophenyl)ethen-1′-yl]-9*H*-carbazole (Cz2PhNO$_2$).* Dry tetrahydrofuran (THF, 5 mL) was added to sodium hydride (NaH, 2.4 g 60% in mineral oil) cooled in an ice bath. To the suspension, a mixed solution of 9-hexyl-3,6-diformyl-9*H*-carbazole (0.5 g, 1.63 mmol) and diethyl (4-nitrobenzyl)phosphonate (0.886 g, 3.42 mmol) in dry THF (5 mL) was added dropwise. The reaction solution was kept stirring at 0 °C for 2 hours. De-ionised water (20 mL) was added, and THF was evaporated with an aspirator. The mixture was dissolved in ethyl acetate (50 mL) and washed with de-ionised water (50 mL) three times, dried over anhydrous magnesium sulfate, and concentrated with an aspirator. Further purification was performed by column chromatography. Yield 84%, mp 255 °C. ^{1}H NMR ($CDCl_3$): δ 0.83 (t, 3H, –CH_3), 1.27 (m, 6H, –CH_2–), 1.85 (quintet, 2H, N–CH_2–CH_2–), 4.30 (t, 2H, –N–CH_2–), 7.16 (d, 1H, J = 16.20 vinyl proton), 7.40 (d, 2H, Ar–*H*, *ortho* to NH), 7.45 (d, 1H, J = 16.32 vinyl proton), 7.63 (d, 2H, Ar–*H*, *meta* to NO_2), 8.21 (d, 2H, Ar–*H*, *ortho* to NO_2), 8.29 (s, 2H, Ar–*H*, *meta* to NH).

Synthesis of poly(ether imide). The details of the synthesis of the diamino monomer and the poly(ether imide) were reported earlier.[26] The poly(ether imide) was acquired after thermal imidization. Dissolving 2,2′-bis(4-aminophenyl)biphenyl (4.11 g, 11 mmol) in dried NMP (15 mL) at 0 °C, 4,4′-(hexafluoroisopropylidene)diphthalic anhydride 6FDA (4.96 g, 11 mmol) was slowly added to the solution. The solution was stirred at room temperature for 2 hours. Adding the solution to methanol dropwise, the polyamic acid was precipitated. The precipitate was washed with methanol and dried over reduced pressure. Thermal imidization was performed at 250 °C for 30 min. Yield 93%, T_g = 220 °C, T_d = 499 °C.

Characterization

Chemical structures were identified by Fourier transform infrared spectra (FT-IR) and ^{1}H NMR spectra. FT-IR spectra were measured with a Bio-Rad FT-IR spectrometer and were performed by mixing samples with KBr powder and pressing the mixture into pellets. ^{1}H NMR spectra were recorded with the use of a INOVA-500 spectrometer, and chemical shifts are reported in ppm units. Thermal transition behaviors were determined by a Seiko SSC/5200 differential scanning calorimeter (DSC) at a heating rate of 10 °C min^{-1}. Thermal degradation temperatures of these compounds were measured by a Seiko 2200 thermogravimetric analyzer (TGA) at a heating rate of 10 °C min^{-1} under nitrogen atmosphere. Linear optical properties were measured with a Perkin-Elmer Lambda UV–Vis spectra. A Metricon 2010 Prism Coupler was utilized to measure refractive indices and thickness of the polymer films. Laser sources were two different wavelengths of He–Ne lasers (543.5 and 632.8) and a diode laser (830 nm).

Thin film preparation. A series of NLO-active poly(ether imide)s containing various chromophore contents were dissolved in spectroscopic grade *N*-methylpyrrolidone (NMP). The solution concentrations were controlled to be about 20 wt%. The solutions were filtered by a 0.22 μm microsyringe. High-quality polymer films were obtained by spin-coating the solution onto indium tin oxide (ITO) coated glass substrates. The spin-coated film was dried at 50 °C for 30 min and then under vacuum at 100 °C overnight.

***In situ* poling.** The corona poling process for the polymer films was carried out using the *in situ* poling technique.[27] The corona discharge was generated from a tungsten wire, which was placed parallel across a 1.0 cm gap above the polymer film. A corona field of 7 kV was applied after the film was heated to

100 °C. The temperature was slowly elevated to 170 °C and then kept at this temperature for 20 min. Finally, the temperature was slowly reduced to room temperature. During poling, the corona current was maintained at 1–2 μA.

Nonlinear optical properties measurement. Second harmonic (SH) coefficients (d_{33}) of the poled films were measured by a Q-switched Nd : YAG laser at 1.064 μm. A Y-cut quartz crystal (d_{11} = 0.5 pm V^{-1}) was used as reference. Relaxation behaviors were investigated by monitoring the decay of the effective SH coefficient, d_{eff}, as a function of time at various temperatures.

Morphology studies. The morphology of the fractured surfaces of the guest–host poly(ether imide)s was characterized by a Hitachi S-4700I high-resolution scanning electron microscope (SEM). The polymer solutions were prepared in the same manner as for spin coating. The solutions were cast onto glass cells and dried at 80 °C for 3 days. To further investigate dispersion of the chromophore in poly(ether imide), an extraction experiment was performed.[28] The cast films can be extracted with or without a co-solvent of acetonitrile and methanol (ratio 3 : 1).

Dielectric analysis. Dielectric relaxation behavior of the NLO guest–host systems was investigated by dielectric spectroscopy using a Novercontrol GmbH equipped with a Schlumberger SI 1260 impedance and gain–phase analyzer as well as a Quator temperature controller. The polymer solutions were prepared in the same manner as for thin film fabrication. The solutions were cast onto the DEA cells and dried at 80 °C for three days. The measured temperature were controlled between −100 °C and +200 °C. The frequency scan range was from 100 mHz to 1 MHz.

Results and discussion

Synthesis and identification of the carbazole–containing chromophore Cz2PhNO$_2$

Scheme 1 depicts the synthetic route of the chromophore. After diformylation of carbazole, the two-dimensional chromophore, Cz2PhNO$_2$, was synthesized *via* a Horner–Emmons–Wadsworth condensation reaction with diethyl (4′-nitrobenzyl)phosphonate. Fig. 2 shows the FT-IR spectrum of the chromophore Cz2PhNO$_2$. Peaks appearing at 1513 and 1339 cm^{-1} contribute from the asymmetric and symmetric stretching bands of nitro groups, respectively. The characteristic stretching band of the conjugated vinyl group appears at 1625 cm^{-1}.

Fig. 3 shows the ^{1}H NMR spectrum of the carbazole-containing chromophore Cz2PhNO$_2$ in deuterochloroform. In the spectrum, the chemical shifts of the vinyl protons appear at 7.16 ppm with a coupling constant of 16.20 Hz, and at 7.45 ppm with a coupling constant of 16.32 Hz. The chemical shifts of the aromatic protons in the nitrophenyl group appear at 7.63 and 8.21 ppm, respectively. Other chemical shifts of the aromatic protons in carbazole are assigned in the spectrum.

The thermal properties of the chromophore Cz2PhNO$_2$ were characterized by DSC and TGA at a heating rate of 10 °C min^{-1} under nitrogen atmosphere. A degradation temperature (T_d; 5 wt% weight loss) was observed at 315 °C in the TGA thermogram. The T_d value is similar to that observed in the DSC thermogram. This high T_d chromophore is more stable than commercially available NLO dyes, such as DO3 (T_d = 235 °C), and DR19 (T_d = 260 °C).[29] Moreover, a melting point

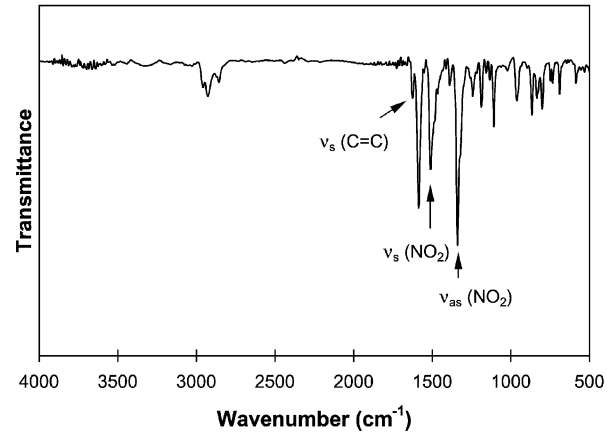

Fig. 2 FT-IR spectrum of the chromophore Cz2PhNO$_2$.

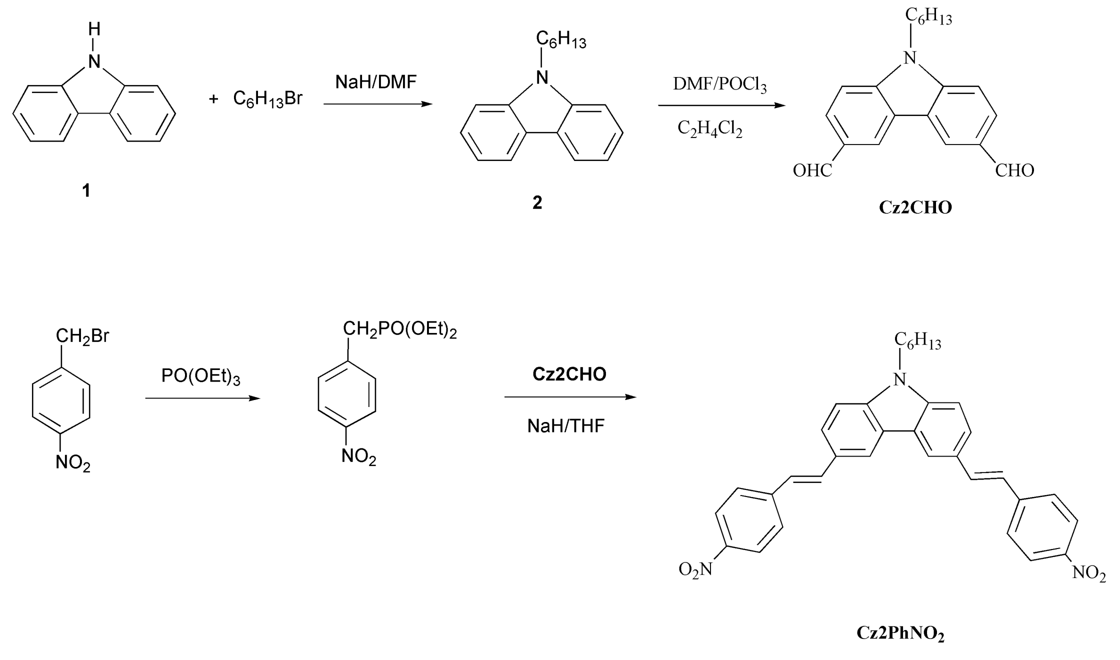

Scheme 1 Synthesis of the carbazole-containing NLO chromophore Cz2PhNO$_2$.

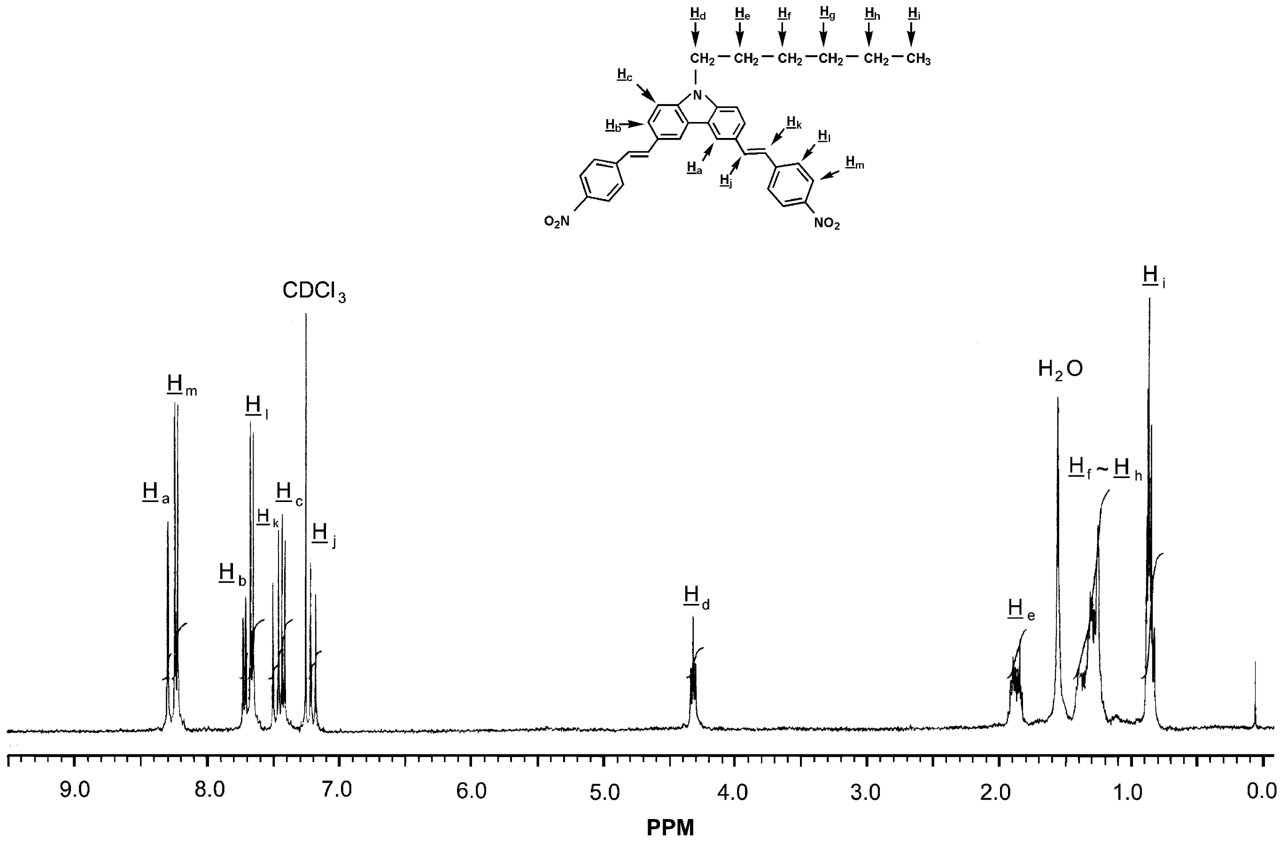

Fig. 3 ^{1}H-NMR spectrum of the chromophore Cz2PhNO$_2$.

(T_m) was found at 255 °C in the DSC thermogram for the chromophore Cz2PhNO$_2$.

Microscopic nonlinearity of the chromophore Cz2PhNO$_2$

The first hyperpolarizability of the chromophore Cz2PhNO$_2$ can be calculated *via* solvatochromic methods.[30] This method is based on the two-state model:[31]

$$\mu_g \beta_{xxx}(2\omega) = \frac{3}{2\hbar^2} \frac{\mu_{eg}^2 \mu_g (\mu_e - \mu_g) \omega_{eg}^2}{(\omega_{eg}^2 - \omega^2)(\omega_{eg}^2 - 4\omega^2)} \qquad (1)$$

where ω_{eg} is the frequency of transition from the ground state to the first excited state, μ_g is the permanent dipole moment of the ground state, μ_e is the permanent dipole moment of the excited state, μ_{eg} is the transition dipole moment between the ground and excited states, and ω is the laser frequency. The frequency of transition, ω_{eg}, can be found simply from the band maximum of the UV–Vis absorption spectrum of the chromophore. The permanent dipole moment of the ground state, μ_g, was obtained from molecular simulation using MOPAC-AM1 optimized geometry.[32] The transition dipole moment, μ_{eg}, is related to the intensity of the transition and can be calculated from the area under the band through eqn. (2):

$$\text{Area} = \int \xi M \mathrm{d}\omega = \frac{2\pi \omega_{eg} N_0 n \mu_{eg} M}{3(2.303)\varepsilon_0 c h} \qquad (2)$$

where M is the concentration of the chromophore, n is the refractive index of the solvent, ξ is the molar absorption coefficient, N_0 is Avogadro's constant, ε_0 is the permittivity of a vacuum, c is speed of light in a vacuum, and h is Planck's constant. Fig. 4 shows the UV–vis absorption spectrum of the chromophore in solvent 1,4-dioxane. Typically the band shape is symmetrical and can be treated as a Lorentzian function. However, various interferences contributed from different conjugated absorptions make the band shape asymmetric at high frequency for long conjugated chromophores. To avoid the interference from other conjugated absorptions, the area of half the absorption band, which did not overlap with other absorptions, was calculated.

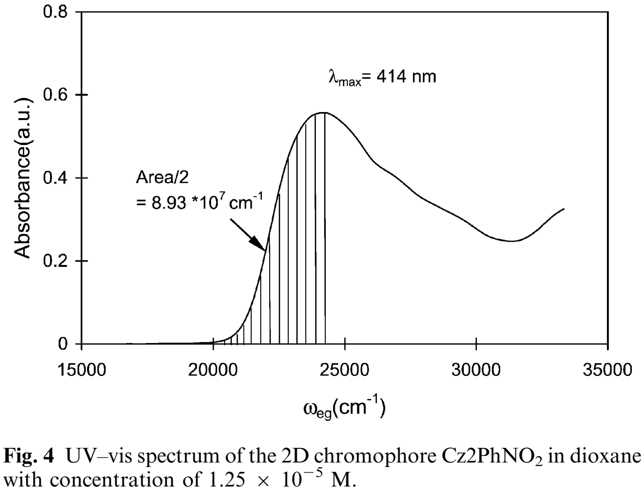

Fig. 4 UV–vis spectrum of the 2D chromophore Cz2PhNO$_2$ in dioxane with concentration of 1.25×10^{-5} M.

Various theoretical treatments of solvatochromic shifts in absorption frequency of the chromophore were developed to determine the permanent dipole moment of the excited state, μ_e. The McRae equation was used to express the solvatochromic shift in this work:[33]

$$(\omega_{eg})_s - \omega_{eg} = A\left[\frac{n^2-1}{2n^2+1}\right] + B\left[\frac{\varepsilon-1}{\varepsilon+2} - \frac{n^2-1}{n^2+2}\right] \qquad (3)$$

$$B = \frac{2}{4\pi\varepsilon_0 \hbar a^3} \mu_g(\mu_g - \mu_e) \qquad (4)$$

where $(\omega_{eg})_s$ is the frequency of the transition in a solvent, ω_{eg} is the frequency of the transition in a vacuum, ε is the relative permittivity of the solvent, and n is the refractive index of the

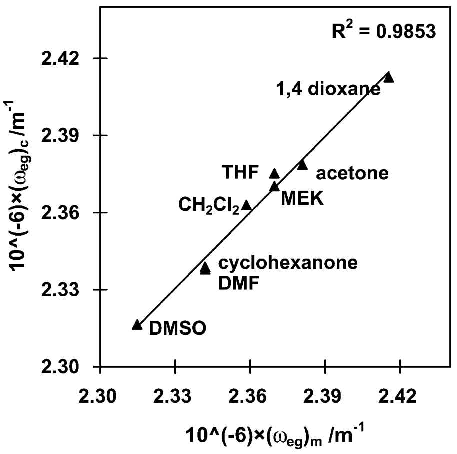

Fig. 5 Solvatochromic fitted curve of the 2D chromophore $Cz2PhNO_2$, where the correlation between measured solvatochromic shift frequency $(\omega_{eg})_m$ and calculated frequency $(\omega_{eg})_c$ from the McRae equation are compared.

solvent. The cavity radius "*a*" can be estimated by various methods. In this work, "*a*" was defined as the length of the conjugated chromophore plus 1.9 Å, whereas the length of the conjugated chromophore was acquired *via* molecular simulation. Fig. 5 shows the representative fit of the solvatochromic shifts to the McRae equation. The data calculated from McRae equation fit well with the experimental data of the solvatochromic shifts. The term $\mu_g(\mu_e - \mu_g)$ was obtained from the fit of the McRae equation. Table 1 shows these solvatochromic data and the first molecular hyperpolarizability (β_{xxx}) of the 2D chromophore $Cz2PhNO_2$.

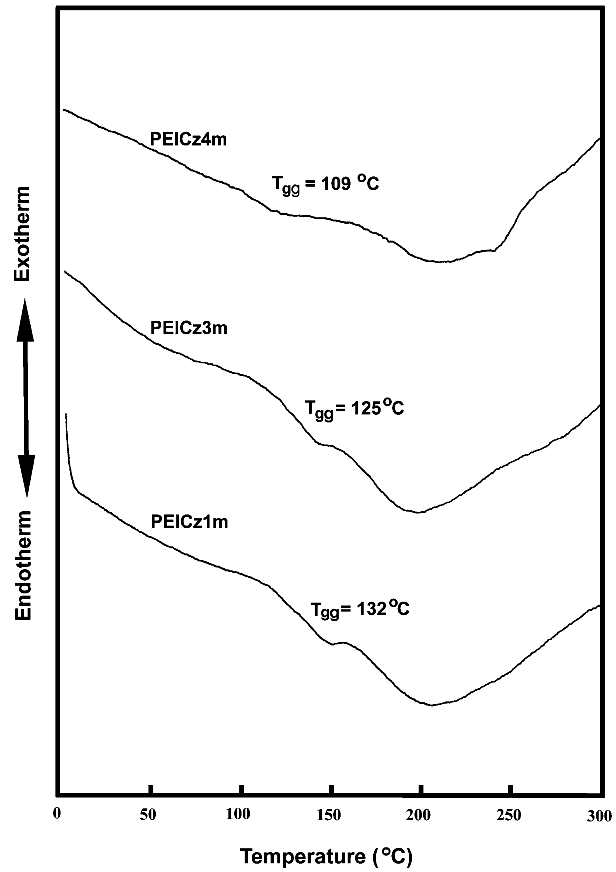

Fig. 6 DSC thermograms of the NLO guest–host poly(ether imide)s PEICzs.

Thermal properties of the guest–host NLO poly(ether imide)s

To investigate the macroscopic NLO properties of the chromophore $Cz2PhNO_2$, an organosoluble poly(ether imide) was used as the polymer matrix. The poly(ether imide) was synthesized according to the literature.[26] The poly(ether imide) possesses excellent solubility in common organic solvents such as NMP, DMF, DMSO, cyclohexanone, THF, and chloroform. An M_w of 38 000 with a polydispersity index of 1.8 was observed. A glass transition temperature (T_g) and degradation temperature with 5 wt% weight loss (T_d) were observed at 220 and 499 °C, respectively. Excellent thermal stability makes this poly(ether imide) suitable as polymer host for NLO chromophores.

By blending 0.1, 0.2, 0.3 and 0.4 mmol of chromophore guest $Cz2PhNO_2$ into in 1 g of poly(ether imide) host, respectively, a series of NLO-active poly(ether imide)s were obtained. They are PEICz1m, PEICz2m, PEICz3m, and PEICz4m in order of increasing chromophore content. The NLO-active poly(ether imide)s were dissolved in NMP and the concentration was controlled at 20% w/v. Excellent quality films were obtained by spin-coating the solution onto ITO glass substrates. No macroscopic phase separation was found in the guest–host systems despite the doping level being as high as 20 wt%. It is important to note that such a high doping level is extraordinary as compared to other guest–host NLO systems.[34,35] This implies that excellent compatibility between poly(ether imide) and chromophore was obtained in this guest–host system.

Fig. 6 shows the DSC thermograms of the guest–host NLO poly(ether imide)s. In the DSC thermograms, transition zones were observed between 75 and 130 °C. The transition temperature decreased as the chromophore content increased. The transition zones could be identified to be the local motion of the biphenoxy group of the polymer backbone by dielectric analysis (DEA). Furthermore, an endothermic peak was found at the higher temperature range in the thermograms. These endothermic peaks may be possibly caused by sublimation of the chromophore $Cz2PhNO_2$. Several techniques were applied to characterize the endothermic peaks and the transition behavior. These include TGA, dielectric analysis, and absorption spectrum under various thermal treatments.

Fig. 7 shows the TGA thermograms of the NLO-active poly(ether imide)s. Three stages of thermal degradation were found. By comparison with the thermograms of the pristine poly(ether imide) and chromophore $Cz2PhNO_2$, the first-stage degradation (180–190 °C) of the guest–host system may be due to sublimation of the chromophore. This sublimation of the chromophore in polymer matrices was identified by detecting UV–vis absorbances at various annealing conditions, which will be discussed in the section 'Optimization of the poling conditions'. This slow first-stage degradation behavior was not

Table 1 Solvatochromic data and first hyperpolarizabilities (β) of the 2D NLO chromophores

	ω_{eg}/cm^{-1}	l^a/Å	$\mu_g{}^a$/D	μ_{eg}/D	μ_e/D	$\beta_{1064}{}^b/10^{-30}$ esu	$\beta_0{}^b/10^{-30}$ esu
$Cz2PhNO_2{}^c$	24154.6	12.981	11.42	12.25	17.02	163.37	54.68

[a] *l* is defined as molecular length, and μ_g is its ground state dipole moment. These data were obtained from molecular simulation using the MOPAC-AM1 geometry method. [b] β_{1064} is defined as β_{xxx} at wavelength 1064 nm, and β_0 as β_{xxx} at infinite wavelength. [c] Solvatochromic data were measured in dioxane solvent.

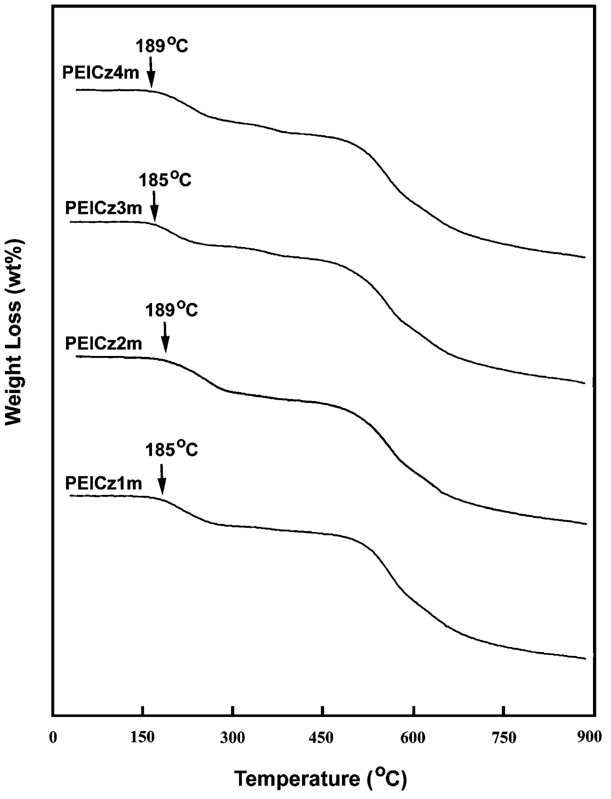

Fig. 7 TGA thermograms of the NLO guest–host poly(ether imide)s PEICzs.

found in the pristine chromophores. This implies that polymer matrices play a role in affecting the degradation behavior of the NLO-active guest–host system. The degree of interaction among the chromophores decreases as the chromophores are doped into polymer matrices. This makes chromophores more susceptible to sublimation at high temperatures.

Optimization of the poling conditions

To obtain the optimized poling temperature and to investigate the sublimation of the chromophore in the guest–host systems, a UV–vis spectrophotometer was utilized to trace the chromophores in the polymer host. Fig. 8 shows the absorption characteristics of the NLO-active poly(ether imide)s thermally treated at various temperatures for 1 h, respectively. No detectable decay of UV intensity was observed after thermal treatment at 170 °C for 50 h. However, a sharp decrease of the absorbance was observed when temperatures were higher than 170 °C. This temperature is slightly higher than the thermal degradation temperatures observed in DSC and TGA thermograms for the guest–host samples. This result indicates that the endothermic peak observed in DSC thermogram and the first-stage degradation in TGA thermogram are caused by the sublimation of chromophores. Similar phenomena have been observed in other literature reports.[36,37] However, thermal treatment experiments and thermal analysis seem not to provide enough information for optimizing poling conditions. In general, the SH signal seems to reach a maximum when the poling temperature approaches the glass transition temperature. However, maximum SH signals were found at *ca.* 150 °C for the NLO-active guest–host system in this work. This shows that the lowest thermal transitions (75–130 °C) found in DSC thermograms are not glass transition temperatures of the NLO-active guest–host poly(ether imide)s. Maximum orientation of the chromophores in the polymer matrices was not achievable at this transition temperature.

On the basis of the above, an optimized poling process was chosen as follows: the polymer films were heated to 120 °C, and then an electric field was switched on. The sample was poled from 120 to 150 °C at a rate of 10 °C h^{-1}. Finally, the poled polymeric film was cooled to room temperature in the presence of the electric field.

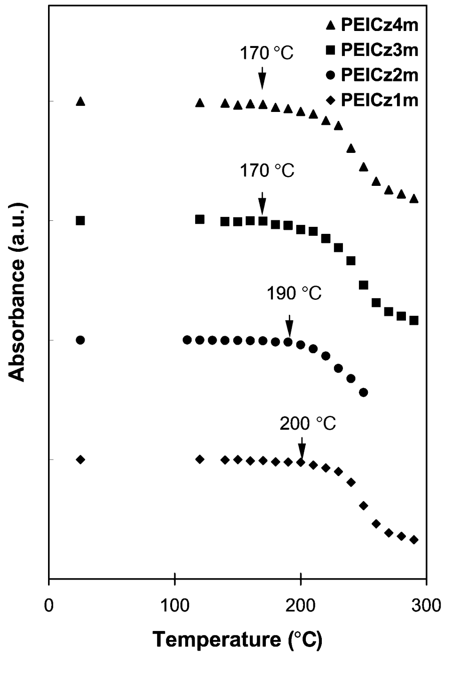

Fig. 8 Thermal stability of the NLO guest–host poly(ether imide)s PEICzs measured using a UV–vis spectrophotometer.

Dielectric analysis

In addition to DSC and TGA thermograms, dielectric spectroscopy is a useful technique for investigating the thermal response of NLO systems because of its high sensitivity to reorientation of the permanent dipole. Fig. 9a and 9b show the temperature dependence of the relative permittivity and dielectric loss tangent for the pristine poly(ether imide) 6FPEI. In the relative permittivity spectrum (Fig. 9a), two relaxation modes, which were assigned as α- and β-relaxation, were found. The α-relaxation corresponding to the glass transition of the poly(ether imide) was observed from 150 to 250 °C. The β-relaxation associated with the rotational motion of the biphenyl ether was located from 50 to 150 °C. In addition to these relaxation modes, a low oscillation strength assigned as γ-relaxation was found at dielectric loss tangent from −100 to 50 °C. The γ-relaxation may be due to local motion of the trifluoromethyl group. Normally rigid polymer backbones would restrict motion of the trifluoromethyl group. This means that the trifluoromethyl group possesses low oscillation strength despite having a strong dipole moment.

Fig. 10 shows the temperature dependence of the relative permittivity and loss tangent for the NLO-active guest–host sample PICz3m. In the relative permittivity spectrum (Fig. 10a), an outstanding α-relaxation was observed from 75 °C to 150 °C. The α-relaxation shifted to lower temperatures and coalesced with the β-peaks for the guest–host PICz3m. A similar phenomenon was observed in the literature.[26] Moreover, the transition observed in DSC thermogram is located in the temperature range. As compared with the discussion in the section 'Optimization of the poling conditions', the transition observed in the DSC thermogram may be due to the motion of the biphenoxy group, *i.e.* β-relaxation. This indicates that the plasticizer effect of the chromophores makes the biphenoxy group more mobile in NLO-active guest–host systems as compared to the pristine poly(ether imide). Similar behavior was found in the DSC thermograms. In Fig. 6, the transition temperature, which is due to local motion of the biphenoxy

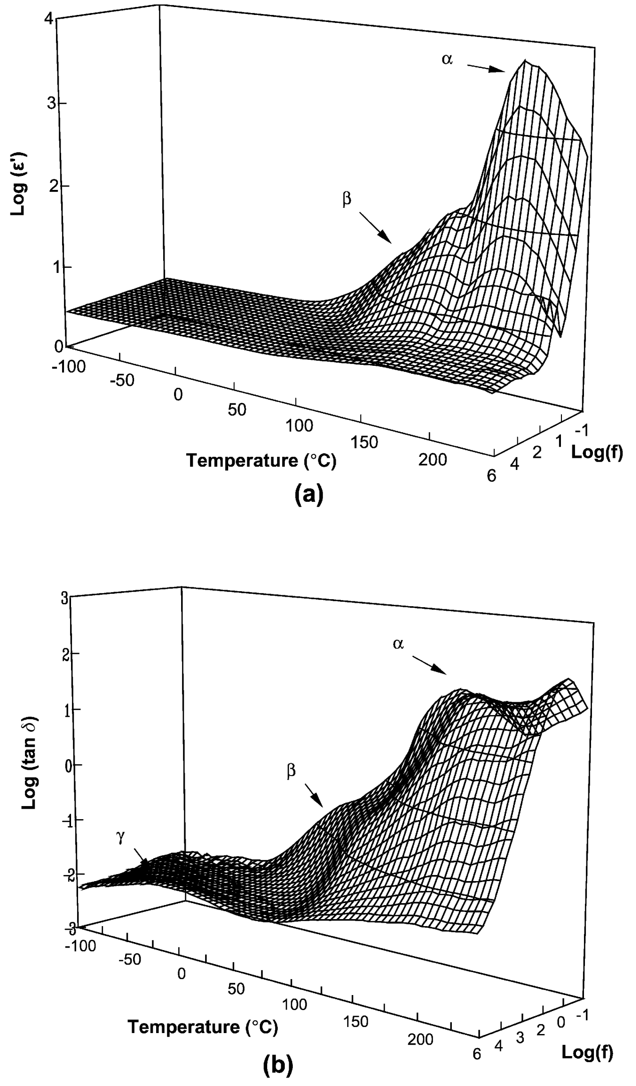

Fig. 9 Dielectric spectra of the pristine poly(ether imide): (a) temperature and frequency dependence of the relative permittivity; (b) temperature and frequency dependence of the tangent δ.

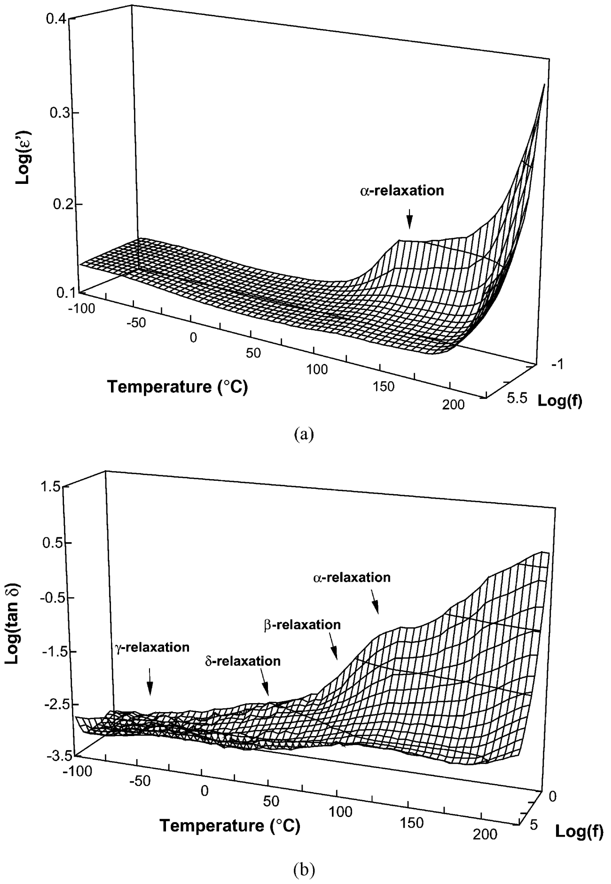

Fig. 10 Dielectric spectra of the NLO poly(ether imide) PICz3m: (a) temperature and frequency dependence of the relative permittivity; (b) temperature and frequency dependence of the tangent δ.

group, is decreased with increasing chromophore content. In the dielectric loss tangent spectrum (Fig. 10b), two local motions were found in addition to the α-relaxation. Compared with the dielectric spectra of the pristine poly(ether imide), a weak σ-relaxation was observed from –50 °C to +40 °C for PEICz3m, which corresponds to the local motion (*i.e.*, crankshaft motion) of the aliphatic chain in the *N*-substituted position of the carbazole. All of the relaxation modes and their corresponding structural motions are shown in Scheme 2.

Morphological analysis

After poling, the polymeric films possess excellent optical transparency even though the chromophore content is up to 20 wt% (PEICz4m). To further investigate the compatibility between the chromophores and poly(ether imide), a high-resolution scanning electron microgram technique was applied. Fig. 11 shows the scanning electron micrographs

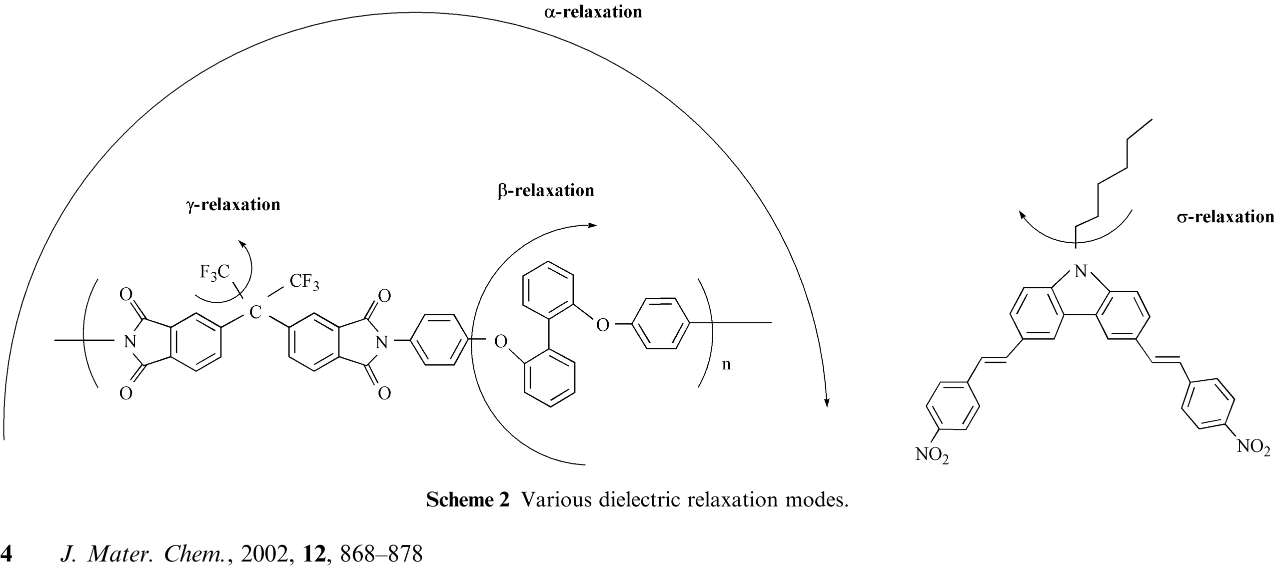

Scheme 2 Various dielectric relaxation modes.

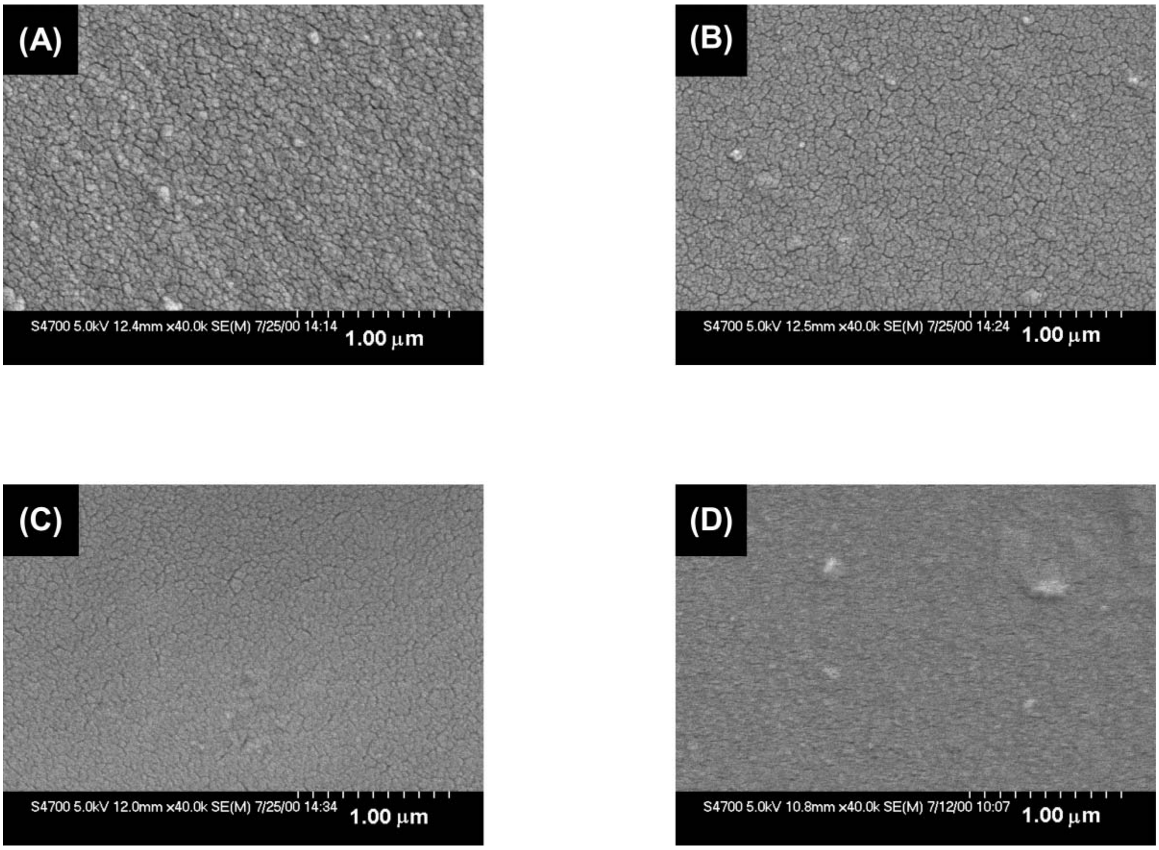

Fig. 11 SEM photographs of the guest–host poly(ether imide)s (A) PEICz1m, (B) PEICz2m, (C) EPICz3m, and (D) PEICz4m.

(× 40K) of the guest–host polymers. Homogeneous fractured surfaces without apparent domains corroborates the excellent compatibility between the chromophores and the poly(ether imide) 6FPEI.

In general, low doping level was the limiting factor for NLO-active guest–host systems owing to the formation of macroscopic phase separation. To further study the factors affecting dispersion of the chromophore Cz2PhNO$_2$ in the poly(ether imide) matrices, the doped polymer films were extracted according to the literature method.[28] A co-solvent of acetonitrile and methanol was used to avoid collapse of the polymer. Fig. 12 shows the scanning electron micrographs (× 7K) of the solvent-treated polymers. The micrographs show droplets (dark section) left in the poly(ether imide) matrices (gray section) after solvent extraction. The droplets may be contributed from dissolution of the chromophores. Compared with untreated films, large size droplets were found in the SEM photographs for the solvent-treated films. Moreover, no phase separation was found in DSC and DEA analysis for the guest–host systems. This implies that the broad polydispersity of poly(ether imide) maybe plays an important role in enhancing compatibility.

Fleer *et al.*[38,39] examined the molecular weight effect of polymers on the interface. They concluded that the shorter chains tend to be in contact with the fillers if the molecular weight distribution is broad. In the previous work, the extracted film and extractant of the sample PICz3m were analyzed *via* GPC. It was found that the low molecular weight part of poly(ether imide)s along with chromophores was extracted and left droplet cavities during solvent treatment. In the continuous phase, higher molecular weight poly(ether imide) is dominant for the polymer matrices. The chromophores present in the continuous phase are constrained by the higher molecular weight poly(ether imide). They cannot be dissolved during the extraction process. Blur interfaces may form owing to the compatibility between high molecular weight and low molecular weight poly(ether imide)s. The blur interfaces elucidate an excellent compatibility between the chromophores and poly(ether imide) matrix.[40]

Linear and nonlinear optical properties

UV–vis absorption spectra of the PEICz3m polymeric film before and after poling are shown in Fig. 13. The maximum absorption wavelength ($\lambda_{\max}$) of polymer PEICz3m appears at 425 nm due to the π–π* transition of the stilbene chromophore. It is noteworthy that little absorbance was found at 532 nm. This shows that low resonance enhancement makes the polymer more useful in electrooptical applications. Fig. 14 shows SH coefficients as a function of chromophore contents. The d_{33} and d_{31} values for the guest–host system PEICzs range from 5 to 22 pm V^{-1} and from 2 to 7 pm V^{-1}, respectively. These SH coefficients increase essentially linearly with increasing chromophore content. This implies that no aggregation of chromophores is present at such a doping level of 20 wt%. Moreover, this further confirms that excellent compatibility is present between poly(ether imide) matrices and chromophores.

The refractive indices of the NLO-active poly(ether imide)s are dominated by the electric absorption spectrum and oscillator strength of the chromophore Cz2PhNO$_2$. Table 2 shows the refractive indices of the NLO-active poly(ether imide)s measured by a Metricon Prism Coupler 2010. The refractive indices of the NLO-active poly(ether imide)s decrease as the wavelength of the operating laser increases. On the other hand the refractive indices of the NLO-active poly(ether imide)s increase as the chromophore content increases. These phenomena can be described by the single oscillation approximation Sellmeier equation (eqn. (5)):[41]

$$n^2 - 1 = \frac{A}{\lambda_{\max}^{-2} - \lambda^{-2}} + B \qquad (5)$$

where $\lambda_{\max}$ is the absorption maximum wavelength, λ is the wavelength at which the refractive index was determined, A is a

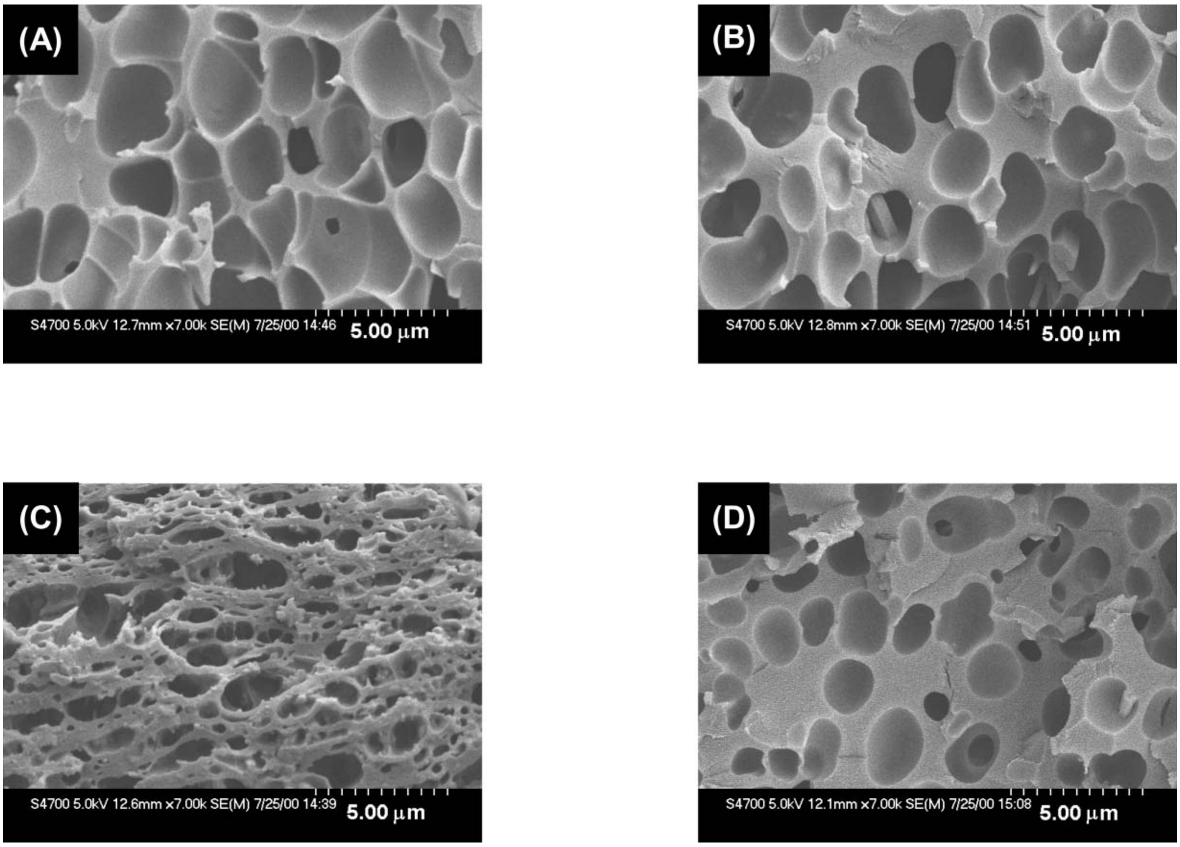

Fig. 12 SEM photographs of the NLO poly(ether imide)s after solvent treatment: (A) PEICz1m, (B) PEICz2m, (C) PEICz3m, and (D) PEICz4m.

constant proportional to the chromophore oscillator strength, and B is all other absorption contributions. The refractive indices of the NLO-active poly(ether imide)s decrease as the wavelength of the operating laser (λ) increases when the chromophore content is maintained constant. Moreover, refractive indices of the NLO-active poly(ether imide)s decrease as the chromophore content increases due to the decrease of chromophore oscillator intensity. This feature is interesting because it provides the opportunity to fine-tune the linear optical properties of the polymers to suit the need for device application.

Temporal relaxation behavior

To investigate the long-term NLO stability of the guest–host systems, dipole reorientation of the aligned chromophores was measured as a function of time. After the optimized poling process, dipole reorientation of the oriented chromophores in the poly(ether imide) matrices was observed by measuring ratios of effective SH coefficients ($d_{\mathrm{eff}}(t)/d_{\mathrm{eff}}(0)$) at various temperatures for a certain period of time.

Fig. 15 and 16 show the time-dependent decay of effective SH coefficient of the NLO guest–host systems at 60 and 80 °C, respectively. In Fig. 15, the effective SH coefficient of the PICzs retained 80–90% of its original value at 60 °C for 200 hours. A fast decay of the effective SH coefficient was observed at the beginning of the thermal treatment, and then the effective SH coefficient remained almost constant. As the temperature was elevated to 80 °C (Fig. 16), a conspicuous decrease in temporal stability was observed as the chromophore content was increased. This phenomenon can be explained by molecular motion from the DEA study mentioned in the previous section.

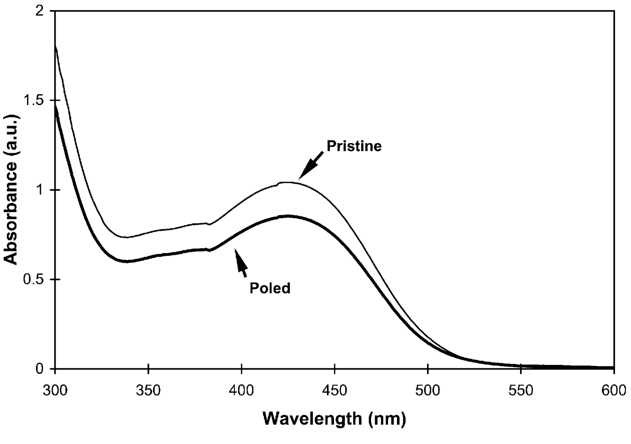

Fig. 13 UV–Vis spectra of the polymer PICz3m before and after the poling process.

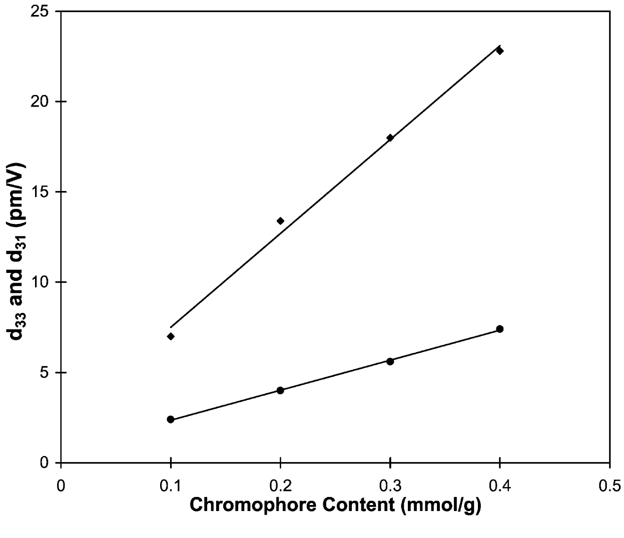

Fig. 14 d_{33}(◆) and d_{31}(●) values as a function of chromophore content per gram of poly(ether imide).

Table 2 Linear and nonlinear optical properties of NLO-active poly(ether imide)s PEICzs

	PEICz1m	PEICz2m	PEICz3m	PEICz4m
$n_{543.5}$[a]	1.636	1.649	1.662	1.674
n_{633}[a]	1.618	1.656	1.635	1.644
n_{830}[a]	1.602	1.639	1.622	1.623
Thickness/μm[b]	0.99	0.91	0.79	0.78
λ_{max}/nm[c]	421	422	425	423
d_{33}/pm V^{-1}	7.0	13.4	18.0	22.8
d_{31}/pm V^{-1}	2.4	4.0	5.6	7.4
Φ[d]	0.24	0.21	0.18	0.18

[a] $n_{543.5}$, n_{633} and n_{830} are defined as the refractive index at wavelength 543.5, 633 and 830 nm, respectively. [b] Thickness of the NLO polymer films. [c] λ_{max} is the maximum absorption wavelength of the NLO films. [d] Φ is the order parameter, which is defined as $(A_0 - A_p)/A_0$, where A_0 is the pristine absorbance, A_p is the absorbance after poling.

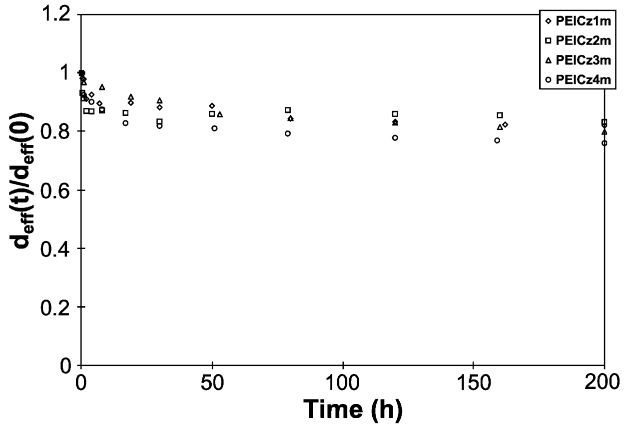

Fig. 15 Time dependence of the dipole reorientation of the NLO polymers PEICz1m, PEICz2m, PEICz3m, and PEICz4m at 60 °C.

Local motion (*i.e.* crankshaft motion) of the aliphatic chain of the chromophore dominates decay of the SH signal when the operating temperature is set at 60 °C. The relaxation of oriented chromophores is confined by the polymer backbone. When the operation temperature is elevated to 80 °C, the rotational motion of the biphenoxy groups would certainly randomize the oriented dipoles.

It is important to note that the SH signal is stable at operating temperatures so close to the temperature range of α-relaxation. Thermal aging possibly contributed to the stabilization of SH signals. More importantly, the structural architecture of the chromophore has a great effect on the temporal stability. In previous literature,[42] a Lackritz's rotational Brownian motion model was utilized to analyze the reorientation of one-dimensional chromophore and two-dimensional chromophores in polymer matrices, respectively. This model describes how the rotational Brownian motion is affected by the electric field and the local mobility of a polymer matrix during and after the poling process. It is assumed that the chromophores can only rotate within a limited space (a rotational cone) because of the highly reduced mobility of the polymer chain in the glass state.[43] In Scheme 3a, the one-dimensional chromophore would rotate around its geometrical center. The dipole moment, μ, is along the major geometrical axis of the chromophore. In this case, the rotational volume is the sum of the two cones. In Scheme 3b, the two-dimensional chromophore can be visualized as wobbling around one end and rotating within one cone. The net dipole moment is normalized to the direction of the two charge transfers. As a result, the rotational cone volume of a two-dimensional chromophore is much larger than that of a one-dimensional chromophore. This large rotational volume retards the randomization of the oriented two-dimensional chromophores in polymer matrices.

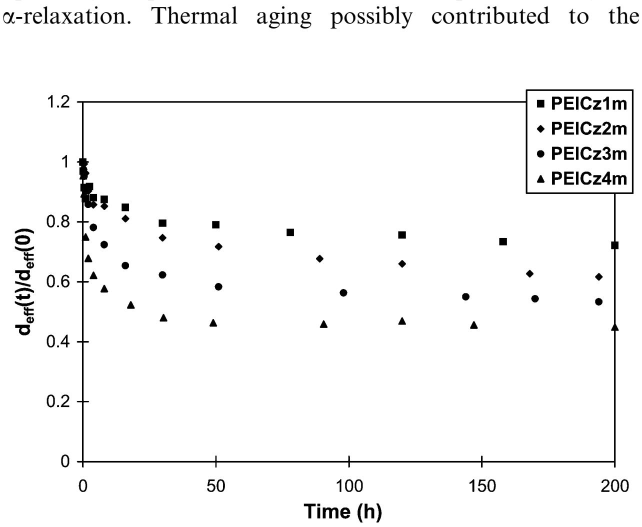

Fig. 16 Time dependence of the dipole reorientation of the NLO polymers (■) PEICz1m, (■) PEICz2m, (●) PEICz3m, and (▲) PEICz4m at 80 °C.

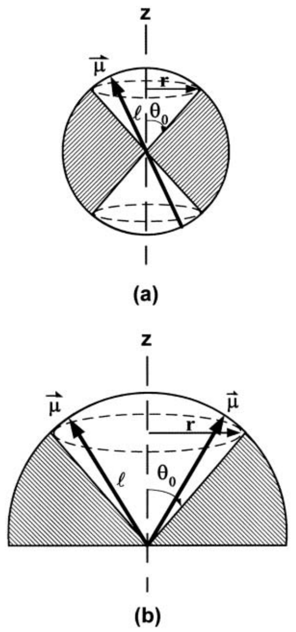

Scheme 3 Schematic diagram of (a) one-dimensional and (b) two-dimensional chromophore rotating in polymer matrix. μ is the dipole moment, l is the axial length of the chromophore, r is the radius of the cross section of the chromophore and θ_0 is the true wedge angle of the chromophore scanning.

A two-dimensional chromophore requires a larger rotational cone volume to randomize than the one-dimensional one. Short-range relaxation such as crankshaft motion cannot provide enough local free volume to randomize the oriented dipoles. As a result, the effective SH coefficient only decays slightly at a low temperature range. As the temperature elevates, long-range relaxation such as biphenoxy segmental motion is allowed to occur. That provides enough local free volume to disorient the poled chromophores. Moreover, the local free volume can be enlarged as the chromophore content is increased (*i.e.*, greater plasticizer effect). Yet, the local free volume surrounding each chromophore was further decreased during an extended poling process.[44] The decrease in the local free volume restricts the dipole reorientation of the chromophore, and induces better temporal stability although the operating temperatures are as high as 80 °C. A similar physical aging effect on the temporal stability of NLO polymers was also observed in the literature.[45–47] These results imply that the rotational volume of the chromophore Cz2PhNO$_2$ is very close to the free volume of the polymer matrices when the operating temperature is close to T_g. This is in contrast to the fast decay of the oriented dipoles of other NLO guest–host systems at temperatures close to T_g.[48–51]

Conclusion

In this work, a two-dimensional chromophore with nitro groups was synthesized. A first molecular hyperpolarizability of 163.4×10^{-30} esu at a wavelength of 1064 nm (β_{1064}) and 54.7×10^{-30} esu at infinite wavelength (β_0) was calculated *via* solvatochromic methods. By doping of the chromophores into an organosoluble poly(ether imide), a series of NLO guest–host materials were obtained. This guest–host system possesses excellent compatibility even though the chromophore content is as high as 20 wt%. Their second harmonic coefficients, d_{33} are in the range of 7–23 pm V^{-1}. In addition to the interaction between the chromophores and the poly(ether imide), the wide molecular weight distribution of the poly(ether imide) plays an important role in promoting the compatibility. A significant feature in enhancing the compatibility in the guest–host systems is the presence of a blur interface. An apparent structural effect on the thermal stability was observed for the two-dimensional chromophore. This two-dimensional chromophore has a large molecular size, which is close to the free volume of the poly(ether imide) during glass transition. The effect of the two-dimensional structure makes the guest–host system possess excellent temporal stability although the operating temperature is close to the glass transition range.

Acknowledgement

The authors thank the National Science Council of Republic of China for financial support of this work (Grant NSC89-2216-E-007-049 and NSC90-2811-E- 007-002). The authors also thank Dr Tein-Fong Hsu and Professor Kuei-Jen Lee for their help in solvatochromic calculation and molecular simulation, respectively.

References

1 P. N. Prasad and D. J. Williams, in *Introduction to Nonlinear Optical Effects in Molecules and Polymers*, John Wiley, New York, 1991.
2 G. A. Lindsay and K. D. Singer, in *Polymers for Second-Order Nonlinear Optics*, ACS, Washington, 1995.
3 W. Wang, D. Chen, H. R. Fetterman, Y. Shi, W. H. Steier, L. R. Dalton and P.-M. D. Chow, *Appl. Phys. Lett.*, 1995, **67**, 1806.
4 F. Li, K. H. Kim, J. J. Kulig, E. P. Savitski, W. J. Brittain, F. W. Harris, S. Z. D. Cheng, S. F. Hubbard and K. D. Singer, *J. Mater. Chem.*, 1995, **5**, 253.
5 N. Nemoto, F. Miyata, Y. Nagase, J. Abe, M. Hasegawa and Y. Shirai, *Macromolecules*, 1996, **29**, 2365.
6 R. D. Miller, D. M. Burland, M. Jurich, V. Y. Lee, C. R. Moylan, J. I. Thackara, R. J. Twieg, T. Verbiest and W. Volksen, *Macromolecules*, 1995, **28**, 4970.
7 G. A. Lindsay, J. D. Stenger-Smith, R. A. Henry, J. M. Hoover and R. A. Nissan, *Macromolecules*, 1992, **25**, 6075.
8 H. E. Katz, K. D. Singer, J. E. Sohn, C. W. Dirk, L. A. King and H. M. Gordon, *J. Am. Chem. Soc.*, 1987, **109**, 6561.
9 L. T. Chen, W. Tam, S. R. Marder, A. E. Stiegman, G. Rikken and C. W. Spangler, *J. Phys. Chem.*, 1991, **95**, 10643.
10 H. Yamamoto, S. Katogi, T. Watanabe, H. Sato, S. Miyata and T. Hosomi, *Appl. Phys. Lett.*, 1992, **60**, 935.
11 K. D. Singer, M. G. Kuzyk and J. E. Sohn, *J. Opt. Soc. Am. B*, 1987, **4**, 968.
12 H. L. Hampsch, J. Yang, G. K. Wong and J. M. Torkelson, *Macromolecules*, 1990, **23**, 3640.
13 M. A. Firestone, M. A. Ratner and T. J. Marks, *Macromolecules*, 1995, **28**, 6296.
14 G. T. Boyd, C. V. Francis, J. E. Trend and D. A. Ender, *J. Opt. Soc. Am. B*, 1991, **8**, 887.
15 V. L. Bell, B. L. Stump and H. Gager, *J. Polym. Sci. Polym. Chem. Ed.*, 1976, **14**, 2275.
16 T. Takekoshi, J. G. Wirth, D. R. Heath, J. E. Kochanocoski, J. S. Manello and M. T. Webber, *J. Polym. Sci. Polym. Chem. Ed.*, 1980, **18**, 3069.
17 W. A. Feld, B. Ramalingam and F. W. Harris, *J. Polym. Sci. Polym. Chem. Ed.*, 1983, **21**, 319.
18 N. D. Ghatge, B. M. Shinde and U. P. Mulik, *J. Polym. Sci. Polym. Chem. Ed.*, 1984, **22**, 3359.
19 Y. Imai, N. N. Maldar and M. Kakimoto, *J. Polym. Sci. Polym. Chem. Ed.*, 1984, **22**, 2189.
20 H. J. Jeong, Y. Oishi, M. Kakimoto and Y. Imai, *J. Polym. Sci. Polym. Chem. Ed.*, 1991, **29**, 39.
21 Y. Qi and Z. Y. Wang, *Macromolecules*, 1996, **29**, 792.
22 B. Kippelen, K. Tamura, N. Peyghambrian, A. B. Padias and H. K. Hall, *J. Phys. Rev.*, 1993, **B48**, 10710.
23 Z. Peng, Z. Bao and L. Yu, *J. Am. Chem. Soc.*, 1994, **116**, 6003.
24 Y. Zhang, S. Ghosal, M. K. Casstevens and R. Burzyaski, *Appl. Phys. Lett.*, 1994, **66**, 2561.
25 H. Hoegl, *J. Phys. Chem.*, 1965, **69**, 755.
26 W. J. Kuo, G. H. Hsiue and R. J. Jeng, *Macromolecules*, 2001, **34**, 2374–2383.
27 M. A. Mortazavi, A. Knoesen, S. T. Kowel, B. G. Higgins and A. Dienes, *J. Opt. Soc. Am. B*, 1989, **6**, 733.
28 H. Veenstra, J. V. Dam and A. P. Boer, *Polymer*, 2000, **41**, 3037.
29 The T_d values of the commercial azo dyes DO3 and DR19 were observed by measuring the onset temperature of the exothermic peak using a Seiko SSC/5200 differential scanning calorimeter and detecting 5 wt% weight loss using a Seiko 2200 thermogravimetric analyzer.
30 M. S. Paley, J. M. Harris, H. Looser, J. C. Baumert, G. C. Bjorklund, D. Jundt and R. J. Tweig, *J. Org. Chem.*, 1989, **54**, 3774.
31 L. DeQuan, M. A. Ratner and T. J. Marks, *J. Am. Chem. Soc.*, 1988, **110**, 1707.
32 E. M. Breitung, C. F. Shu and R. J. McMahon, *J. Am. Chem. Soc.*, 2000, **122**, 1154.
33 E. G. McRae, *J. Phys. Chem.*, 1957, **61**, 562.
34 K. D. Singer and L. A. King, *J. Appl. Phys.*, 1991, **70**, 3251.
35 K. Y. Wong and A. K. Y. Jen, *J. Appl. Phys.*, 1994, **75**, 3308.
36 Y. C. Shu, Z. H. Gong, C. F. Shu, E. M. Breitung, R. J. McMahon, G. H. Lee and A. K. Y. Jen, *Chem. Mater.*, 1999, **11**, 1628.
37 M. A. Pauley, H. W. Guan and C. H. Wang, *J. Chem. Phys.*, 1996, **104**, 6834.
38 G. J. Fleer, M. A. Cohen Stuart, J. M. H. M. Scheutjens, T. Cosgrove and B. Vincent, *Polymers at Interfaces*, Chapman & Hall, London, 1993.
39 L. H. Sperling, *Polymeric Multicomponent Materials: an Introduction*, John Wiley & Sons, New York, 1997.
40 R. A. L. Jones and R. W. Richards, *Polymers at Surfaces and Interfaces*, Cambridge University Press, Cambridge, 1999.
41 I. McCulloch, G. Boudoughian and H. T. Man, *Adv. Mater.*, 1995, **7**, 715.
42 L. Y. Liu, D. Ramkrishna and H. S. Lackritz, *Macromolecules*, 1994, **27**, 5987.
43 C. Wang and R. Pecora, *J. Chem. Phys.*, 1980, **72**, 5333.
44 T. III Goodson, S. S. Gong and C. H. Wang, *Macromolecules*, 1994, **27**, 4278.
45 H. L. Hampsch, J. Yang, G. K. Wong and J. M. Torkelson, *Macromolecules*, 1990, **23**, 3648.
46 S. C. Lee, A. Kidoguchi, T. Watanabe, H. Yamamoto, T. Hosomi and S. Miyata, *Polym. J.*, 1991, **23**, 1209.
47 J. S. Royl and J. M. Torkelson, *Macromolecules*, 1993, **26**, 5331.
48 Y. Shi, W. H. Steier, M. Chen, L. Yu and L. R. Dalton, *Appl. Phys. Lett.*, 1992, **60**, 2577.
49 C. A. Walsh, D. M. Burland, V. Y. Lee, R. D. Miller, B. A. Smith, R. J. Tweig and W. Volksen, *Macromolecules*, 1993, **26**, 3720.
50 J. I. Chen, S. Marturunkakul, L. Li, R. J. Jeng, J. Kumar and S. K. Tripathy, *Macromolecules*, 1993, **26**, 7379.
51 N. Tsutsumi, S. Yoshizaki, W. Sakai and T. Kiyotsukuri, *Macromolecules*, 1995, **28**, 6437.